

# Adaptive Active Contour Model for Brain Tumor Segmentation

Gunjan Naik, University of Pune, India\*

Aditya Abhyankar, Savitribai Phule Pune University, India

Bhushan Garware, Persistent Systems, India

Shubhangi Kelkar, Persistent Systems, India

## ABSTRACT

For accurately diagnosing the severity of brain tumors in MRI images, Glioma segmentation is a significant step. The Glioma segmentation is due to noise and weak edges of organs in medical images. The geodesic active contour model (GACM) is a standard method for the segmentation of complex organ structures based on edge maps. The GACM performs poorly due to this noise and weak edges. So, the authors propose a method that uses adaptive kernels instead of a constant kernel for creating strong edge maps for GACM. The kernels used in phase congruency are Log Gabor kernels, which resemble similar anisotropic properties like Gabor kernels. They have replaced these with adaptive kernels. This adaptive kernel-based phase congruency provides a robust edge map to be used in GACM. Experimentation shows that when compared with state-of-the-art edge detection techniques, adaptive kernels enhance the weak as well as strong edges and improve the overall performance. Moreover, the proposed methodology substantially requires fewer parameters compared to existing ACM methods.

## KEYWORDS

Active Contour Model, GACM, ICA, Kernel, Medical Image Segmentation, Phase Congruency

## 1. INTRODUCTION

Medical image segmentation is a method for partitioning or distinguishing organ boundaries in medical images. Although traditionally, radiologists use experience and judgment to perform diagnostics, automatic and semi-automatic image segmentation methods are needed to assist them.

For medical images like CT scans, exposure of radiation is in the range of 1 mSv(millisievert) up to 15 mSv. Within this range, the harm to the patient's body is minimal. However, prolonged exposure to CT scans can be hazardous. So, MRI images are more preferred for soft tissues (Images, n.d.). As our work is focused on Glioma segmentation, we have preferred MRI data. The dataset used for our experimentation is from the BRATS competition (Menze et al., 2014).

Even though MRI provides details of tissues, they still suffer from weak edges for gliomas. Image segmentation of these weak edges is challenging as thresholding methods may fail (Global

DOI: 10.4018/IJCVIP.314947

\*Corresponding Author

This article published as an Open Access article distributed under the terms of the Creative Commons Attribution License (<http://creativecommons.org/licenses/by/4.0/>) which permits unrestricted use, distribution, and production in any medium, provided the author of the original work and original publication source are properly credited.

thresholding, n.d.). Researchers have used Active methods for segmentation for these kinds of weak boundary problems.

Active methods are based on the philosophy of curve evolution and they are called active, because, the curves in these methods dynamically alter their shape and position while seeking a minimal energy state (Kass et al., 1988). Active methods are categorized into two parts: template-based methods and seed-based methods.

In active methods, there are template-based methods which is used to segment organs with a well-defined structured shape, size, and texture of organs. The template-based methods such as the active shape model (ASM) (Cootes et al., 1995) and the active appearance model (AAM) (Cootes et al., 1998), are based on statistical models of shapes and appearance (texture). Using training data, these models learn about the variation of shape and appearance. The curves of these models alter their shape to fit an example of the object for a new image. So, template-based methods are mainly used in areas like knee segmentation (Vincent et al., 2010), liver segmentation (Heimann et al., 2006).

The seed-based methods need seed point to create contours or initial entry points. The first seed-based method is Kass's Active contour method (ACM). ACM is based on the energy minimization principle. The total energy is defined by, 'internal energy' which is based on the initialization of contour and 'external energy' is defined utilizing image properties of the object of interest. Generally, external energy is based on an edge map, which stops on the boundary of the object. The edge map is generated using a constant gradient kernel is used, like Prewitt, Sobel, and Canny. The Gradient kernels are constant kernels and due to which the modelling of weak edges is not satisfactory.

To get a robust segmentation, ACM requires an edge map with strong edges, else the contour boundaries do not stop at ROI during evolution. Though most of the research in literature is towards proposing new methodologies of curve evolution or Internal energy. Research on external energy definition is mostly based on, use of constant kernel edge detector. The constant kernel edge detector fails to capture weak edges, hence there is a need to develop methods to extract a robust edge map.

In this paper, we have proposed a novel biologically vision inspired method based on Adaptive kernels extracted using Independent Component Analysis (ICA) for extracting an edge map. The ICA-based Adaptive kernels in phase congruency methods are used along with Phase congruency, to create robust edge maps. These edge maps when compared with other traditional edge detection techniques to define external energy for GACM, has improved the segmentation performance of Active methods.

For experimentation, we have used the BRATS dataset (Menze et al., 2014) of brain tumors for Glioma (Brain tumor) segmentation. However, as this approach is not based on the Deep learning approach, we have not compared it with current Deep learning methods present on BRATS' leaderboard.

The remainder of this paper is as follows: The contribution of our paper is explained in 1.1. The proposed methodology is discussed in 3 and based on the methodology experiments are shown in 3.1. Finally, we discussed the conclusions and future scope in section 4.

## 1.1 Our Contribution

Here, we have proposed an adaptive kernel framework for active methods in which, the mask or kernel will be learned from images with less manual intervention.

The ICA bases give a response like a Gabor wavelet (Lee, 1996) when convolved with a given image. While using the Gabor wavelet, the Gabor kernel is modified by the manual setting of parameters like scale, frequency, and orientation, as per the required anisotropic properties. But, in the case of ICA, the basis is having learned scale, frequency, and orientation. The ICA bases when convolved with a given image, generate texture maps in different directions and strengths. These textures are linearly separable, so the extracted texture maps can be combined by summation operation. ICA-based kernels not only found strong edges but also weak edges. These weak edges, when added to the original image, enhance the original image, which will be used for GACM.

We have also proposed a method in which, we have used ICA-based kernels for the Phase congruency method by (Kovesi, 1999). Phase is an important property of an image (Huang et al., 1975); however, most of the edge detection techniques are based on intensity values. Phase congruency is based on phases extracted using sine and cosine filters present for edge detection. For using sine and cosine components, log Gabor kernels (Fischer et al., 2007) are used. As these log Gabor kernels are constant kernels, which do not consider image information of a given image; we have replaced Log Gabor kernels with ICA kernels.

## 2. RELATED WORK

### 2.1 Adaptive Kernels

The concept of the adaptive kernel was proposed by, Olshausen and field (1996). In their study of the visual synapses the brain, they have created a mathematical model of the receptive fields. This mathematical model gives a set of codes which are called sparse codes, as they are active only for only some regions. The sparse codes are proposed to create a dictionary, which can be used for image coding and compression, which can have receptive fields similar to humans. The human receptive field is the first section of the visual cortex. The visual cortex is divided into 5 categories. The part of the visual cortex that receives the sensory inputs from the thalamus is the number one visible cortex, additionally recognized as visible area 1 (V1), and the striate cortex. The extra-striate regions consist of visible regions 2 (V2), three (V3), 4 (V4), and 5 (V5). The V1 area is for extracting the edges, curves from a given picture. whereas, the V2 to V5 are for complicated operations, like creating a structure from edges and knowledge of it.

The sparse codes extracted by Olshausen and field are similar to the receptive fields present in V1. Ideally, these sparse codes should be localized, oriented, bandpass. However, these properties were not satisfied with the methodology proposed by Olshausen and Field.

Based on the theory of independent component analysis (ICA), which was proposed by Aapo Hyvarinen (2000), the sparse codes should have statistical independent properties. Although ICA has been proposed to solve the problem of source separation (BSS), it can be used to extract Adaptive kernels.

### 2.2. Active Contour Model

The first ACM or snake algorithm was proposed by Kass (1988), which is defined using the geometric properties of contour and image content. In Kass ACM, external energy is defined with two factors: 1) the combination of the forces due to the image itself, in simple terms it the edge strength of the boundaries and 2) the constraint forces introduced by the user.

The combination of forces for Kass ACM is nothing but the edge strength of the given image. This edge strength is calculated by constant kernel gradient operators like Prewitt (1970), Sobel (2012), and Canny (1986). After this, snake or contour lock onto the nearby edges and localize them.

However, Kass ACM cannot handle topology changes and is unable to evolve on a convex shape, due to first and second-order derivative functions. So, to handle topology changes, a new methodology was proposed by (Caselles et al., 1997) named Geodesic active contour.

In Geodesic active contour, the internal energy is based on Riemannian space. So, this method is also called the geometric active contour model. The geometric active contour model or geodesic active contour model (GACM) is the ACM that can split, and merge based on the interior and exterior region. The contour evolution is based on the geodesic distance in the Riemannian space. The convergence criterion of ACM and GACM is generally defined using a gradient-based edge map, using which the contour gets locked on the nearby edges.

Instead of a gradient operator, (Xu & Prince, 1998) proposed a gradient vector flow function, to define external energy for the ACM. The significance of gradient vector flow is that it aids to

process difficult boundary cavities. But gradient vector flow is again depending on the edge strength of the boundaries, which will fail for weak boundaries. Chan and Vese (2002) proposed a method for ACM, without using edge information. They have proposed to have a mean curvature motion and Mumford Shah model for defining energy of the contour. This model evolves the contour based on the internal and external region, so, stopping criteria does not depend on the gradient of the image. However, the Chan Vese method is used mostly for foreground and background subtraction and cannot segment a particular object of interest.

The general ACM methodology relies upon the quality of edges. These edges are calculated using constant kernel gradient operators. However, these gradient operators are having low sensitivity for weak edges and are unable to capture directional information in all directions. The fundamental problem with the gradient operator is that they have a fixed kernel, which considers directional information only for two directions: vertical and horizontal. Due to this, they are very poor in localizing an edge, and thus chances of finding a false edge or loss of a weak edge are higher. So, to capture directional (Anisotropic) information in more directions, multiresolution approaches have been proposed.

For capturing directional information, multiresolution methods like Wavelet have been proposed by (Liu & Hwang, 2003), which use the wavelet transform to have directional information in three directions namely vertical, horizontal, and diagonal. (Shan & Ma, 2010) proposed to use a curvelet to define the external energy for active contour. Curvelet transform is used to have a set of kernels, in more than three directions, which localizes edges effectively than wavelet transform.

C. Sagiv (2006) proposed to use of Gabor filters in the GACM theory. Gabor kernels are modeled as simple cells in the visual cortex. Gabor wavelet is used to find the texture and as an edge indicator function using the Beltrami framework as a submanifold. This submanifold is having a Riemannian structure that forms full spatial feature space. The determinant of the manifold is treated as a gradient in Gabor space. Gabor filters provide visual information in combined form as frequency and space.

(Xu et al., 2020) proposed to use signed pressure force function, whereas (Joshi et al., 2021) defined global signed pressure and K-means clustering based on local correntropy with the exponential family (GSLCE) for external energy definition. Another pressure force function has been proposed (Liu et al., 2020).

A density-based methodology has been proposed in (Yin et al., 2020) which deals with density-oriented BIRCH (balanced iterative reducing and clustering using hierarchies) clustering method. (Han & Wu, 2020) proposed a new local and global active contour model based on Jereys divergence. (Niaz et al., 2020) formulates by combining the statistical information of both the local and global region-based energy fitting models.

The edge preservation method technique for ACM (Jiang & Jiang, 2020) is based on matrix factorization and the use of local spectral histograms. However, the edge detection is not consistent as the calculation of the local histogram is highly parametric. Also, it is based on intensity-based edge preservation, hence weak edges cannot be modelled. All the above methods are based on intensity values or in the spatial domain, which is not sufficient to model the weak edges. The weak edge modeling is more suitable for phase values or in the frequency domain.

### 2.3 Phase Congruency

Methods based on the local energy models (Concetta Morrone & Burr, 1988), like Phase congruency (Esteves et al., 2012) are based on phase values for edge detection. Phase congruency has been used for external energy creation (Cinar et al., 2017), (Karn et al., 2018). However, in this approach to capture required directional information using multiresolution methods, parameters like scale, space, and orientation must be tuned for log Gabor kernels. This tuning is done by brute force and judgment. So, instead of tuning the parameters, we have proposed to improve the weak edges employing Adaptive kernels and then compare the performance with previous methods.

Though deep learning methods for edge detection have been developed recently (Xie & Tu, 2015),(Liu et al., 2019),(Soria et al., 2020); our approach is based on shallow learning. So, we are not comparing results with deep learning methods. Due to shallow learning (Chauhan et al., 2019), the computational power required for our method is less, which is another requirement for hospitals in the Indian subcontinent.

### 3. PROPOSED METHODOLOGY

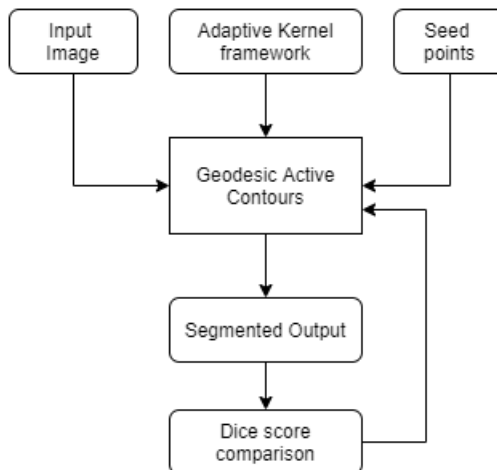
As shown in Fig. 1, ACM requires that seed points are placed around the region of interest. These seed points are joined into a single contour or multiple contours. These contours are then grown or evolved based on the energy minimization principle.

Before energy minimization, the energy of contour should be first defined using the attributes of contour and image properties. The energy of the contour is distinguished into two parts: internal energy and external energy. Internal energy is used to control the movement of the contour. External energy controls how the contour gets attracted to the image boundary. The contour evolves along the direction and magnitude of the sum of internal energy and external energy. After defining energy, the energy is minimized using gradient descent which decides the rate of contour evolution. This energy minimization results in contour evolution. In simple terms, the energy of the contour is the magnitude with which the contour points shift towards the object of interest. The energy minimization performs the contour shrinking to get a boundary.

This contour evolution rate should decrease near the boundaries such that it will finally stop at the boundary. However, to stop the contour evolution at the boundary, either the parameters chosen should be selected with extreme care or the boundary should be well defined. As the convergence or stopping criteria of ACM depends on the boundary or edge, external energy is an important entity in contour evolution. External energy is generally defined using the edge map of the given image. These edge maps are extracted using a constant kernel method.

Researchers have proposed different techniques to define, internal and external energy of the contour. Our approach is to define external energy in a robust way for strong as well as weak edges, with the consideration of the philosophy of Directional Filter Bank (Bamberger & Smith, 1992) and adaptive kernels. Instead of using Gabor kernels as it is, we have learned kernels that have similar

Figure 1. Adaptive kernel framework block diagram



Anisotropic properties like Gabor kernel. These kernels are learned from statistical properties of image or set of image patches is necessary, because these kernels find directional information in all directions, to extract strong as well as weak edges. These kernels are called Adaptive kernels as they evolve as per the image. The algorithm is mentioned in fig 2.

We have proposed to use the ICA kernels to improve the edge strength. Also, we have used the isotropic information extracted using ICA with the Phase congruency method, which results in improved boundary extraction as intensity and phase information are combined.

### 3.1 ICA Based Edge Detection

Using the theory of Adaptive kernels, an image can be represented as a linear combination of basis, as follows:

$$x = \sum_{i=0}^{N-1} A_i \cdot y_i = A_0 \cdot y_0 + A_1 \cdot y_1 + A_2 \cdot y_2 + \dots + A_{N-1} \cdot y_{N-1} \quad (1)$$

Here,  $A_i$  is the  $i^{\text{th}}$  basis function, and  $y_i$  is the coefficient. [1] can be written as:

$$x = A \cdot y \quad (2)$$

where  $y$  is a coefficient vector,  $y_i$  is an element of  $y$ , and the weighted coefficient of projecting a patch image into the  $i^{\text{th}}$  basis function ' $A_i$ '. ' $A$ ' is a matrix of ICA basis functions and  $A_i$  is the  $i^{\text{th}}$  column vector of the ICA basis matrix.

As we want to find edges, we should address the local part of the image. So, we will extract the patches. We have to find the sources or basis present from the image patches, such that combining only the source part will result in an edge map. As we have to find sources or bases for images, this problem can be solved as a blind source separation problem. i.e., the information of sources is not

Figure 2. Algorithmic steps

---

**Algorithm 1:** Adaptive kernel based ICA for edge detection for improvement for Geodesic Active contour

---

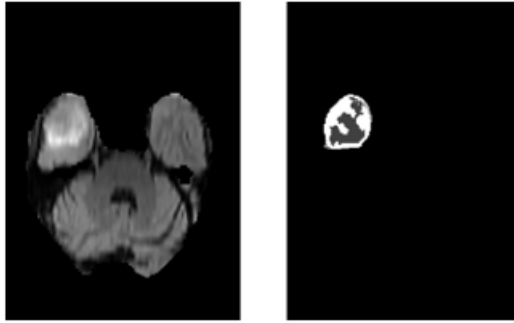
```

1 ICA based Adaptive kernels for Glioma improvement
   Input : Input image, Seed points,
           Ground-truth, Advection, Curvature,
           Propagation
   Output: Segmented output, Dice_score_final
2 dice_score_final=0
3 for i= 0 to number of iterations
4 dice_score=dice_cal_function(Ground-
  truth,Segmented output)
5 if i = 0 and dice_score_final equals dice_score then
6 | dice_score_final = dice_score ;
7 else if i not equal to 0 and dice_score_final less than
  dice_score then
8 | dice_score_final = dice_score ;
9 | Update Advection, Curvature, Propagation ;
10 else
11 | dice_score_final = dice_score ;
12 end

```

---

Figure 3. Input image (Brain tumor MRI) along with its annotation of Tumor



known prior. The ICA is performed by finding a matrix  $W$  which estimates the coefficients  $y$  being as statistically as independent as possible over data  $x$ , as shown in eq [3]:

$$y = W \cdot x \quad (3)$$

The ICA components  $y$  may be permuted and rescaled. For that, a neural learning algorithm for ICA was proposed in (Bell & Sejnowski, 1995) and (Bell & Sejnowski, 1997), in which the joint entropy is maximized by using a stochastic gradient ascent. The updating formula for  $W$  is:

$$\Delta W = \left( I + g(y) \cdot y^T \right) \cdot W \quad (4)$$

where,  $T$  represents the transformation of a matrix;  $y=W \times x$ , the transformation function of the coefficient vector for  $y$  is  $g(y) = \frac{2}{(1 + \exp^{-y})}$ . The input data should be normalized and so whitening is performed for that using eq [5]:

$$x = W_0 \cdot (x - m_x) \quad (5)$$

So, the new transformation is done using a product of the whitening matrix and learned matrix, as shown in eq. 6:

$$W_I = W \cdot W_0 \quad (6)$$

After the transformation, the basis needs to be completed and orthogonal, so the ICA transformation matrix  $W_I$  needs to be orthogonalized using eq. [7]:

$$W = W_I \cdot \left( W_I^T \cdot W_I \right)^{-\frac{1}{2}} \quad (7)$$

As edge detection is performed using High pass filtering, where edges are high changes in intensity. So, selecting proper bases can be selected using sparsity values; which can be found using eq. 8:

$$\|A_i\| = \left( \sum_{j=0}^{N-1} (|a_{ij}|^p) \right)^{\frac{1}{p}} \quad (8)$$

where  $p < 1$ .

This is  $l_p$  norm, where  $A_i$  ( $i=0, 1, 2, 3, \dots, N-1$ ) is the  $i^{\text{th}}$  basis function and  $A_{ij}$  is the  $j^{\text{th}}$  coefficient of  $i^{\text{th}}$  basis. The smaller the value of  $A_i$ , the sparsity will be more. If  $A_i=0$ , then that base is completely sparse. The ICA bases are rearranged according to sparseness value and then components with low sparsity are ignored.

After finding out the ICA basis, these ICA bases are multiplied with the given image patches. These transformed patches are reconstructed, and we get texture maps for each kernel:

$$\begin{aligned} \text{texture map}_m &= \sum_{i=m}^{N-1} A_i \cdot y_i \\ &= A_m \cdot y_m + A_{m+1} \cdot y_{m+1} + \dots + A_{N-1} \cdot y_{N-1} \end{aligned} \quad (9)$$

where  $m$  is the number of basis functions, should be greater than or equal to 1.

Using eq. 9, we have to remove the components with edges at different orientations by comparing sparsity values.

For a given image the image patches are extracted with the patch size of '8'. These patches are converted into a single row vector and then stacked into a matrix. This is the  $y$  matrix as discussed in eq [2]. After this, the ICA algorithm is applied to this as per equations [5] to [7]. These procedures give us 64 basis functions, as shown in fig. 4.

As you can see in fig 5, all basis functions are not localized and oriented. Some bases are showing low pass properties. However, the value of other basis elements is varied and can be larger and smaller in zero local range; the value of another place is near to zero. As edge detection is performed using High pass filtering, where edges are high changes in intensity. So, selecting proper bases with high pass property will do edge detection. These bases can be selected using sparsity values; which can be found using eq [8].

After finding out the ICA basis, these ICA bases are convolved with the given image patches. These transformed patches are reconstructed, and we get texture maps for each kernel. If all texture maps are added, then the original image will get reconstructed. As we have to find an edge map, we

Figure 4. 64 ICA kernels

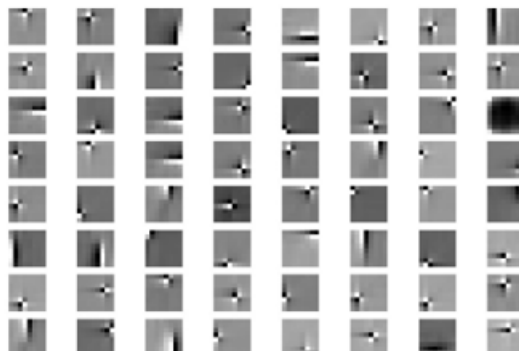


Figure 5. Convolution output with kernels



have to drop the isotropic texture maps. After dropping the isotropic part, the remaining texture maps should be added. After taking absolute values of this texture map using eq. [9], we will get the edge map of a given image as shown in fig 3. We have also shown the original image along with its Canny output. Thus, we are getting a good edge map in terms of covering all the components. But instead of using an edge map for natural images, we have experimented on a medical dataset of the BRATS competition. We have compared our method with canny edge detection with the help of an overlap measure of annotation and extracted image segment. We also considered medical image enhancement methods proposed by Perona (1990) and Nyul (2000). Perona proposed a diffusion-based method of anisotropic diffusion, where a Gaussian kernel is diffused to enhance strong edges and remove weak edges. As tumor edges are mostly weak edges compared to other brain components, anisotropic diffusion is not used. Whereas, in Nyul normalization, the basic requirement is training data should be there to find the percentiles. The percentiles are required to find the histogram of all the images and how it is distributed. Based on these percentiles, the images are enhanced in a given image range using interpolation. But this method is highly parametric and also tedious to improve weak as well as strong edges. As this method learns percentiles using all the data, our method improves the edge information without the need for complete training data.

### 3.2 ICA Based Phase Congruency

Our proposed work is also involved in the incorporation of Phase information using ICA kernels and Phase congruency, to find weak boundaries of glioma. The use of only intensity values for finding weak edges in segmentation makes the problem a bit challenging. So, experimentation has been done based on phase-based edge detection. The phase-in image is defined as the change in intensity values while going from x-direction or y-direction.

Phase congruency is a method based on the local energy model, proposed by Morrone. This model is based on thresholding in the frequency domain. The given image is transformed into the frequency domain using Fourier transform. In the frequency domain, the edge will have all the Fourier components in phase. Thus, the component is said to be congruent, and hence phase congruency value is maximum at edges:

$$PC(x) = \frac{\max_{\phi(x) \in [0, 2\pi]} \sum_n A_n \cdot \cos(\phi_n(x) - \bar{\phi})}{\sum_n A_n} \quad (10)$$

where  $A_n$  is the amplitude of nth Fourier component of a 1D signal  $I(x) = \sum_n A_n \cos \phi_n(x)$ .

$\phi_n$  is local phase component.

Though Phase congruency calculation in the 1D domain is simple using eq [10], the calculation in 2D is complicated.

Peter Kovessi simplified the calculation in images, by proposing the use of a filter bank of quadrature logarithmic filter. Here, there are two filters namely odd and even filters are used for this method, which is 90° phase-shifted from each other. This phase shift is based on Hilbert transform approximation. Their definitions are as follows:

$$F(x) = \sum_n I(x) \cdot M_n^e \quad (11)$$

$$H(x) = \sum_n I(x) \cdot M_n^o \quad (12)$$

where,  $M_n^e$  is even filter and  $M_n^o$  is odd filter.

The sum of amplitudes of frequency component in F(x) is given by:

$$\sum_n A_n(x) = \sum_n \sqrt{(I(x) \cdot M_n^e)^2 + (I(x) \cdot M_n^o)^2} \quad (13)$$

Using the above equations [11],[12],[13], the Phase congruency was defined as:

$$PC(x) = \frac{E(x)}{\sum_n A_n(x) + \epsilon} \quad (14)$$

where  $E(x) = \sqrt{F(x)^2 + H(x)^2}$  is a small constant for preventing the eq [14], becoming unstable. Phase congruency used Log Gabor filters to perform edge detection. The Log Gabor filters proposed by Field (1987), are an alternative to the Gabor function. Field suggests that natural images are better coded by filters that have Gaussian transfer functions when viewed on the logarithmic frequency scale. On the linear frequency scale, the log-Gabor function has a transfer function of the form:

$$G(w) = e^{-\log\left(\frac{w}{w_0}\right)^2} \cdot \frac{2^{(\log(\frac{k}{w_0}))^2}}{w_0} \quad (15)$$

where,  $w_0$  is the filter's center frequency  $\frac{k}{w_0}$  must also be held constant for varying  $w_0$ , such that the filters will get constant shape for edge detection. In our experiment, we replace the even filter ( $M_n^e$ ) and the odd ( $M_n^o$ ) filter with the ICA kernel. As the ICA components are extracted from the image and changes for each image, this methodology is termed as Adaptive Phase congruency.

As the first adaptive kernel after finding sparsity values is carrying the information about intensity changes. This kernel resembles the isotropic properties of the Log Gabor kernel. The even filter used

in Phase congruency is calculated on the assumption that the log Gabor component is present in that image. As ICA kernels extracted from the given image, using ICA kernels instead of constant Log Gabor kernels is justifiable. Based on this hypothesis, we have done experimentation for glioma segmentation. The results of which are discussed in the next section.

#### 4. EXPERIMENTATION

We have considered the BRATS database of brain tumor segmentation to compare the results of the Canny edge detector and ICA-based edge detector with the Geodesic Active contour method. The evaluation metric used is the dice score which is the overlap between the annotated image segment and image segment extracted from the image segmentation algorithm. The formula for dice score is:

$$Dice\ score = \frac{2|A \cap B|}{|A| + |B|}$$

where  $|A \cap B|$  represents the common elements between sets A and B, and  $|A|$  represents the number of elements in set A (and likewise for set B).

In the BRATS database, the labels are provided for different tumor regions. These regions are evaluated based on the region of the tumor i.e., complete tumor, core tumor, and enhanced tumor. Also, there are 4 modalities present in this dataset, namely T1, T2, T1C, and Flair. Due to four modalities, the problem becomes four-channel single-segmented output with multiple classes.

To reduce the complexity of the problem, we evaluated our algorithm for a full tumor, as an initial challenge. The Full tumor is visible in the Flair modality, so we have performed our experimentation on the Flair modality only. Now the underlying problem becomes a two-class pixel classification or binary class problem with a single-channel image, where the classes are tumor and non-tumor.

Instead of using the traditional active contour method. We have used 'Geodesic Active contour' with level sets. The geodesic active contour model requires two inputs along with parameter tuning. The two inputs are a seed image and an edge map. The seed points are extracted based on the labels provided in the database and kept the same for all the methods. The parameter tuning is a crucial part as the finding of the optimal parameter varies according to the edge map. To have a fair comparison of the mentioned algorithms, these parameters are tuned using the particle swarm optimization method. These methods are applied with the same range of parameters for geodesic active contour and, to get the optimum results.

The tumor is having minute intensity variations along with it, so they are having weak edges compared to other brain components. The methods like anisotropic diffusion are used for improving the strength of strong edges, but it removes all the weak edges, which is not desirable. Whereas, the ICA edge map extracts all the relevant edges i.e., weak as well as strong edges. We added those edges in the original image and normalized the edges, such that the difference in the strength of weak edges and strong edges is minimal. The result of geodesic active contour using Canny edge detection is shown in 6.

The results in the figure 6 show that the edges are not clear enough after performing canny edge detection. Whereas, in figure 7, the change in the frequency of tumor boundary is getting improved. Due to which, we get crisp edges of the tumor. These edges are improving the overall performance of the Geodesic active contour method.

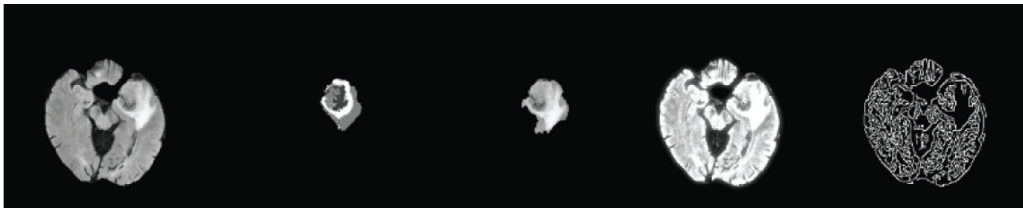
We have compared our results on BRATS 2013 dataset with 20 patients of high-grade glioma (HGG) and 10 patients of low-grade glioma (LGG), from training data. Each MRI contains around 150 slices each. For having the same contrast ratio with a matched histogram, there is another method named Nyul normalization. Nyul normalization performs histogram matching by first finding percentiles

Figure 6. Tumor segmentation using canny edge detection



*Dice score=0.785: (from left to right) original image, annotated part, extracted tumor, canny edge map*

Figure 7. Tumor segmentation for ICA with canny



*Dice score=0.909: (from left to right) original image, annotated part, extracted tumor using proposed method, ICA improved edge map, canny edge map*

and then interpolate them. This is a widely used method for MRI histogram normalization. Nyul method requires a training phase, to find percentiles in the image, and then this phase will be used to transform the image into a normalized domain. Whereas, our method does not require a specific training phase and can be used in cases where data is less. We have compared the GACM with Canny edge detector, Canny with Nyul normalization, and ICA-based edge detection. The comparison of results is in table 1.

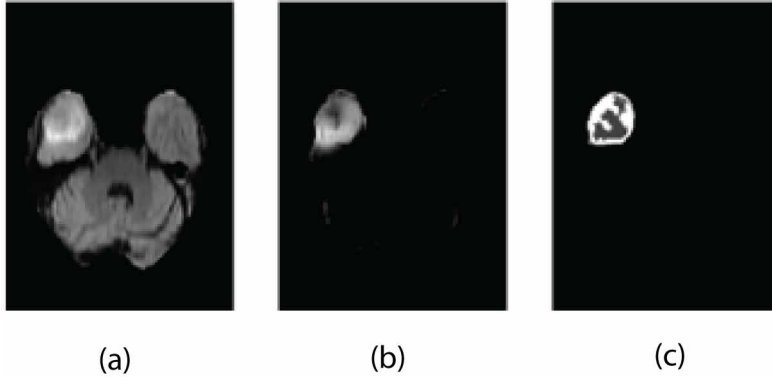
After the use of ICA edge information to improve the weak edges of the tumor, the next stage was to use ICA based Phase congruency model. This method is based on incorporating adaptive kernel from ICA instead of Log Gabor kernel. The output of Adaptive Phase congruency is shown in figure (4).

As shown in above figure 8, the tumor region can be extracted with a good edge difference. But, still, there is some pre-processing needed to remove the outer boundary of the brain, as it is also gets considered as an edge. Though the segmented output and manually annotated output is having a high dice score (around 0.9), for comparison with other techniques, we have used the GACM pipeline along with ICA-based Phase congruency. After combining, the adaptive kernel on ICA, we have used this output for Geodesic Active contour methodology, to incorporate intensity information along with curvature also. The results are compared with the Canny and traditional Phase congruency model.

Table 1. Comparison of Canny edge, Nyul normalization and ICA edge operator with GACM

Glioma Type	Canny edge operator	Nyul Normalization	ICA edge operator
LGG	0.758	0.785	0.803
HGG	0.669	0.703	0.708
Average Dice score	0.714	0.744	0.756

Figure 8. (a) Given image; (b) ICA based Phase congruency output; (c) Manual annotation



For checking if the improved results are consistently better every time, we have recalculated the seed points and calculated the dice calculation for 4 methods, which are, Canny edge detector, ICA based edge detection, Phase congruency with Log Gabor kernels, and Phase Congruency with ICA based kernels. The results are in table 2.

The results of ICA-based edge detection and ICA-based Phase congruency, are much better than Canny and Phase congruency methods. The box plot for the given output is shown in Figure 9.

The box plot for Low-grade glioma is as shown in the above figure. As you can see the traditional methods for external energy are having a low median value when compared to ICA based adaptive

Table 2. Comparison of Canny, ICA edge detection, Phase congruency and ICA based Phase congruency

Glioma type	Canny edge operator	ICA edge operator	Phase congruency	ICA phase congruency
LGG	0.783	0.810	0.799	0.839
HGG	0.729	0.783	0.781	0.797
Average Dice score	0.756	0.797	0.790	0.818

Figure 9. Box plot for LGG

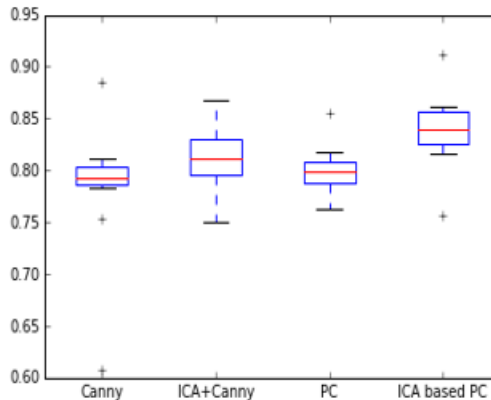
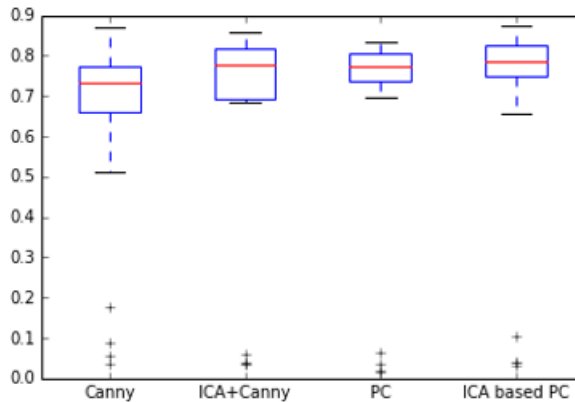


Figure 10. Box plot for HGG



kernel method. As the tumor edges are weak for the LGG case, the adaptive kernel method can boost the weak edges. Thus, there is a good improvement in the overall dice score.

Ideally, the box plot shown in fig 10, should have fewer outliers, and the width of the box should be small. The box plots are showing these characteristics when compared to traditional methods. As the tumor boundaries are quite visible in High-grade cases, the improvement in dice score is minimal when compared to LGG. After looking at both LGG and HGG cases, we can observe that the overall performance has improved with fewer outliers.

## 5. CONCLUSION

The adaptive kernel-based method proposed in this paper improves the performances of Glioma segmentation by robustly detecting weak edges. Weak edges are difficult to capture because of very minute intensity variation. Earlier methods use constant kernels to solve the segmentation problem, whereas, the proposed method based on biological vision, adaptively generates kernels for each image using Independent Component Analysis.

For initial experimentation, ICA-based kernels are used to perform edge detection. However, the next experiments are performed along with Phase congruency. The incorporation of image-specific kernels instead of Log Gabor kernels, in the Phase congruency method, improves the segmentation performance by accurately separating the Glioma boundary.

We have compared adaptive kernel-based edge detection techniques with Canny and Phase congruency, for defining the external energy of Geodesic Active contour. The adaptive kernel-based edge detection techniques have shown an improved average dice score of 0.979 (ICA edge detection), 0.818 (ICA-based Phase congruency) compared to 0.756 (Canny), 0.790 (Phase congruency).

In the future, we propose to investigate, if Adaptive Phase congruency can be used in other segmentation domains like aerial image segmentation, carotid ultrasound segmentation (Azzopardi et al., 2020). Deep learning losses based on Active contour (Tan et al., 2021) can be modified by incorporating Adaptive phase congruency.

## ACKNOWLEDGMENT

This research is funded by Prime Minister Fellowship for Doctoral research, with Persistent System Ltd. as Industry partner and Department of Technology, Savitribai Phule Pune University as Academic Partner.

## REFERENCES

- Azzopardi, C., Camilleri, K. P., & Hicks, Y. A. (2020). Bimodal automated carotid ultrasound segmentation using geometrically constrained deep neural networks. *IEEE Journal of Biomedical and Health Informatics*, 24(4), 1004–1015. doi:10.1109/JBHI.2020.2965088 PMID:31944969
- Bamberger, R. H., & Smith, M. J. (1992). A filter bank for the directional decomposition of images: Theory and design. *IEEE Transactions on Signal Processing*, 40(4), 882–893. doi:10.1109/78.127960
- Bell & Sejnowski. (1997). The independent components of natural scenes are edge filters. *Vision Research*, 37(23), 3327–3338.
- Bell, A. J., & Sejnowski, T. J. (1995). An information-maximization approach to blind separation and blind deconvolution. *Neural Computation*, 7(6), 1129–1159. doi:10.1162/neco.1995.7.6.1129 PMID:7584893
- Canny, J. (1986). A computational approach to edge detection. *IEEE Transactions on Pattern Analysis and Machine Intelligence*, PAMI-8(6), 679–698. doi:10.1109/TPAMI.1986.4767851 PMID:21869365
- Caselles, Kimmel, & Sapiro. (1997). Geodesic active contours. *International Journal of Computer Vision*, 22(1), 61–79.
- Chauhan, S., Vig, L., De Filippo De Grazia, M., Corbetta, M., Ahmad, S., & Zorzi, M. (2019). A comparison of shallow and deep learning methods for predicting cognitive performance of stroke patients from MRI lesion images. *Frontiers in Neuroinformatics*, 13, 53. doi:10.3389/fninf.2019.00053 PMID:31417388
- Chen, Y.-W., Zeng, X.-Y., & Lu, H. (2002). *Edge detection and texture segmentation based on independent component analysis*. In *Object recognition supported by user interaction for service robots* (Vol. 3). IEEE.
- Cinar, A., Barhli, S., Hollis, D., Flansbjerg, M., Tomlinson, R., Marrow, T., & Mostafavi, M. (2017). An autonomous surface discontinuity detection and quantification method by digital image correlation and phase congruency. *Optics and Lasers in Engineering*, 96, 94–106. doi:10.1016/j.optlaseng.2017.04.010
- Concetta Morrone, M., & Burr, D. (1988). Feature detection in human vision: A phase-dependent energy model. *Proceedings of the Royal Society of London. Series B, Biological Sciences*, 235(1280), 221–245. doi:10.1098/rspb.1988.0073 PMID:2907382
- Cootes, T. F., Edwards, G. J., & Taylor, C. J. (1998). Active appearance models. In *European conference on computer vision* (pp. 484–498). Springer.
- Cootes, T. F., Taylor, C. J., Cooper, D. H., & Graham, J. (1995). Active shape models—their training and application. *Computer Vision and Image Understanding*, 61(1), 38–59. doi:10.1006/cviu.1995.1004
- Esteves, T., Quelhas, P., Mendonca, A. M., & Campilho, A. (2012). Gradient convergence filters and a phase congruency approach for in vivo cell nuclei detection. *Machine Vision and Applications*, 23(4), 623–638. doi:10.1007/s00138-012-0407-7
- Field. (1987). Relations between the statistics of natural images and the response properties of cortical cells. *Josa A*, 4(12), 2379–2394.
- Fischer, S., Sroubek, F., Perrinet, L., Redondo, R., & Cristobal, G. (2007). Self-invertible 2d log gabor wavelets. *International Journal of Computer Vision*, 75(2), 231–246. doi:10.1007/s11263-006-0026-8
- Global thresholding: An overview. (n.d.). <https://www.sciencedirect.com/topics/engineering/global-thresholding>
- Han, B., & Wu, Y. (2020). Active contour model for inhomogeneous image segmentation based on Jeffreys divergence. *Pattern Recognition*, 107, 107520. doi:10.1016/j.patcog.2020.107520
- Heimann, T., Wolf, I., & Meinzer, H.-P. (2006). Active shape models for a fully automated 3d segmentation of the liver—an evaluation on clinical data. In *International Conference on Medical Image Computing and Computer-Assisted Intervention* (pp. 41–48). Springer. doi:10.1007/11866763\_6
- Huang, T., Burnett, J., & Deczky, A. (1975, December). The importance of phase in image processing filters. *IEEE Transactions on Signal Processing*, 23(6), 529–542. doi:10.1109/TASSP.1975.1162738

Hyvarinen, J., & Oja, E. (2000). Independent component analysis: Algorithms and applications. *Neural Networks*, 13(4), 411–430. PMID:10946390

Images, H. (n.d.). *MRI vs. CT scan | health images*. <https://www.healthimages.com/mri-vs-ct-scan>

Jiang, J., & Jiang, X. L. (2020). An improved matrix factorization based active contours combining edge preservation for image segmentation. *IEEE Access: Practical Innovations, Open Solutions*, 8, 223472–223481. doi:10.1109/ACCESS.2020.3044881

Joshi, A., Khan, M. S., Niaz, A., Akram, F., Song, H. C., & Choi, K. N. (2021). Active contour model with adaptive weighted function for robust image segmentation under biased conditions. *Expert Systems with Applications*, 175, 114811. doi:10.1016/j.eswa.2021.114811

Karn, P. K., Biswal, B., & Samantaray, S. R. (2018). Robust retinal blood vessel segmentation using hybrid active contour model. *IET Image Processing*, 13(3), 440–450. doi:10.1049/iet-ipr.2018.5413

Kass, M., Witkin, A., & Terzopoulos, D. (1988). Snakes: Active contour models. *International Journal of Computer Vision*, 1(4), 321–331. doi:10.1007/BF00133570

Kovesi, P. (1999). Image features from phase congruency. *Videre: Journal of Computer Vision Research*, 1(3), 1–26.

Lee, T. S. (1996). Image representation using 2d gabor wavelets. *IEEE Transactions on Pattern Analysis and Machine Intelligence*, 18(10), 959–971. doi:10.1109/34.541406

Liu, Fang, Zhang, & Lin. (2020). A novel active contour model guided by global and local signed energy-based pressure force. *IEEE Access*, 8, 59412–59426.

Liu & Hwang. (2003). Active contour model using wavelet modulus for object segmentation and tracking in video sequences. *International Journal of Wavelets, Multiresolution and Information Processing*, 1(1), 93–113.

Liu, Y., Cheng, M.-M., Hu, X., Bian, J.-W., Zhang, L., Bai, X., & Tang, J. (2019, August). Richer convolutional features for edge detection. *IEEE Transactions on Pattern Analysis and Machine Intelligence*, 41(8), 1939–1946. doi:10.1109/TPAMI.2018.2878849 PMID:30387723

Menze, B. H., Jakab, A., Bauer, S., Kalpathy-Cramer, J., Farahani, K., Kirby, J., Burren, Y., Porz, N., Slotboom, J., Wiest, R., Lanczi, L., Gerstner, E., Weber, M.-A., Arbel, T., Avants, B. B., Ayache, N., Buendia, P., Collins, D. L., Cordier, N., & Van Leemput, K. et al. (2014). The multimodal brain tumor image segmentation benchmark (brats). *IEEE Transactions on Medical Imaging*, 34(10), 1993–2024. doi:10.1109/TMI.2014.2377694 PMID:25494501

Niaz, Rana, Joshi, Munir, Kim, Song, & Choi. (2020). Hybrid active contour based on local and global statistics parameterized by weight coefficients for inhomogeneous image segmentation. *IEEE Access*, 8, 57348–57362.

Nyul, L. G., Udupa, J. K., & Zhang, X. (2000). New variants of a method of mri scale standardization. *IEEE Transactions on Medical Imaging*, 19(2), 143–150. doi:10.1109/42.836373 PMID:10784285

Olshausen, B. A., & Field, D. J. (1996). Emergence of simple-cell receptive field properties by learning a sparse code for natural images. *Nature*, 381(6583), 607–609. doi:10.1038/381607a0 PMID:8637596

Perona, P., & Malik, J. (1990). Scale-space and edge detection using anisotropic diffusion. *IEEE Transactions on Pattern Analysis and Machine Intelligence*, 12(7), 629–639. doi:10.1109/34.56205

Prewitt, J. M. (1970). Object enhancement and extraction. *Picture Processing and Psychopictorics*, 10(1), 15–19.

Sagiv, C., Sochen, N. A., & Zeevi, Y. Y. (2006). Integrated active contours for texture segmentation. *IEEE Transactions on Image Processing*, 15(6), 1633–1646. doi:10.1109/TIP.2006.871133 PMID:16764287

Seger, O. (2012). Generalized and separable sobel operators. *Machine vision for three-dimensional scenes*, 347.

Shan, H., & Ma, J. (2010). Curvelet-based geodesic snakes for image segmentation with multiple objects. *Pattern Recognition Letters*, 31(5), 355–360. doi:10.1016/j.patrec.2009.10.018

Soria, Riba, & Sappa. (2020). *Dense extreme inception network: Towards a robust CNN model for edge detection*. Academic Press.

Tan, L., Ma, W., Xia, J., & Sarker, S. (2021). Multimodal magnetic resonance image brain tumor segmentation based on acu-net network. *IEEE Access: Practical Innovations, Open Solutions*, 9, 14608–14618. doi:10.1109/ACCESS.2021.3052514

Vincent, Wolstenholme, Scott, & Bowes. (2010). Fully automatic segmentation of the knee joint using active appearance models. *Medical Image Analysis for the Clinic: A Grand Challenge*, 1, 224.

Xie & Tu. (2015). *Holistically-nested edge detection*. Academic Press.

Xu, C., & Prince, J. L. (1998). Snakes, shapes, and gradient vector flow. *IEEE Transactions on Image Processing*, 7(3), 359–369. doi:10.1109/83.661186 PMID:18276256

Xu, L., Zhu, Y., Zhang, Y., & Yang, H. (2020). Liver segmentation based on region growing and level set active contour model with new signed pressure force function. *Optik (Stuttgart)*, 202, 163705. doi:10.1016/j.ijleo.2019.163705

Yin, Li, Liu, & Karim. (2020). Active contour modal based on density-oriented birch clustering method for medical image segmentation. *Multimedia Tools and Applications*, 79(41), 31049-31068.